Inorganica Chimica Acta 428 (2015) 176–184

Contents lists available at ScienceDirect

Inorganica Chimica Acta

journal homepage: www.elsevier.com/locate/ica

Synthesis and the characterization of Schiff-base copper complexes: Reactivity with DNA, 4-NPP and BNPP

Natalia Kozlyuk, Tyler Lopez, Patrick Roth, J. Henry Acquaye *

Department of Chemistry, University of Redlands, 1200 East Colton Avenue, Redlands, CA 92373, United States

ARTICLE INFO

Article history:
Received 10 October 2014
Received in revised form 12 December 2014
Accepted 17 December 2014
Available online 7 February 2015

Keywords:
Schiff-base ligands
Copper complexes
Crystal structures
DNA interaction
BNPP and 4-NPP cleavages

ABSTRACT

Two new copper Schiff-base complexes have been synthesized and characterized by use of spectroscopic techniques. The Schiff-base ligands, (*E*)-*N*-((1-methyl-1*H*-imidazol-2-yl)methylene)quinolin-8-amine, MICQ and (*E*)-1-((quinolin-8-ylimino)methyl)naphthalen-2-ol, TL1 were obtained from the reaction of 8-aminoquinoline with 1-methyl-2-imidazolecarboxaldehyde and 2-hydroxy-1-napthaldehyde respectively. The reaction of MICQ with copper(II) chloride produced complex **1**, [Cu(MICQ)Cl](PF_6), whereas the reaction of TL1 with copper(II) acetate resulted in complex **2**, Cu(TL1)(OAc)·CH_3OH. The single crystal X-ray structure determination of both complexes show distorted square planar geometries around the copper center. The reactivity of the complexes with calf thymus DNA, CT-DNA and plasmid DNA have been studied using ethidium bromide displacement fluorescence emission, electronic absorption spectroscopy and agarose gel electrophoresis analysis. From the fluorescence emission studies K_{sv} values of $3.70 \times 10^3\ M^{-1}$ and $7.82 \times 10^3\ M^{-1}$ were obtained for complexes **1** and **2**, respectively. The absorption titration resulted in K_b values of $1.52 \times 10^5\ M^{-1}$ for complex **1** and $5.00 \times 10^5\ M^{-1}$ for complex **2**. The results indicate that both complexes significantly interact with CT-DNA and also show cleavage of supercoiled DNA. In addition, complex **2** was found to hydrolyze the DNA model compounds bis(4-nitrophenyl) phosphate, BNPP and 4-nitrophenyl phosphate, 4-NPP.

1. Introduction

The interaction of transition-metal complexes [1–5] with DNA continues to attract interest in the search for anticancer chemotherapeutic agents due to the success of cisplatin [6]. Cisplatin is currently used in the treatment of a number of malignancies including testicular and ovarian cancer. Despite its worldwide use and success in such treatment, the drug has been found to have serious side effects such as liver toxicity, nausea and vomiting and development of drug resistance. These shortfalls have stimulated researchers to develop new and effective alternatives to cisplatin. Copper complexes are in the forefront of that search. The biochemical activity of copper in many biological systems makes it a good choice for use as chemotherapeutic drug [7,8]. During the past few decades, several copper complexes have been synthesized and studied for their interaction with DNA [9–25]. Metal complex–DNA interactions can be classified as intercalation, electrostatic binding, covalent binding and hydrolytic cleavage. Several copper complexes have been found to exhibit these modes of interaction. Furthermore, a number of the copper complexes have been found to exhibit cytotoxicity levels that are comparable to or greater than that of cisplatin [26–39].

Among the various modes of interactions of metal complexes with DNA, the hydrolysis of phosphate ester bonds in DNA serves as one important reaction for DNA degradation [40,41]. The DNA backbone consists of phosphate ester bonds, which impart high stability to the DNA framework. The half-life of the phosphodiester bond in DNA is estimated to be 130000 years. Hence the hydrolysis of the phosphodiester bonds in DNA is kinetically a slow process under normal physiological conditions. The stability of the phosphodiester bonds in DNA is considered to be nature's mechanism to safeguard the stability of the genetic make-up of life forms. In many biological systems, metalloenzymes catalyze the hydrolysis of the very stable phosphodiester bonds [42,43]. The phosphohydrolases generally contain Zn, Mg, Fe, Mn or Ni. Several studies have been conducted with Cu(II) complexes for the hydrolysis of phosphodiester bonds [44–49]. The hydrolysis of phosphodiester bonds and phosphate monoester bonds in model compounds such as bis(4-nitrophenyl) phosphate (BNPP) and 4-nitrophenyl phosphate (4-NPP) respectively constitute important reactions for understanding the reactivity of metalloenzymes and metal complexes with DNA. Metal complexes imitating hydroxylases could serve as possible chemotherapeutic anti cancer agents. The devel-

* Corresponding author.

http://dx.doi.org/10.1016/j.ica.2014.12.034
0020-1693/

opment of metal complexes that could function as metalloenzymes has therefore been the focus of several researchers [46–49,50–53].

The type of ligands attached to the metal center generally influences the reactivity of a metal-based chemotherapeutic drug. Varying the ligands could tune the reactivity of the complex towards DNA. Planar ligands with pi systems have been noted to be good intercalators [54–58]. The planarity of such ligands contributes to the intercalating mode of binding of the complex to DNA. Copper complexes have been shown to interact non-covalently with DNA if they contain planar aromatic ring ligands capable of inserting between the DNA base pairs. A significant example is the work done by Sigman and co-workers [59] that led to the discovery that the copper complex $[Cu(phen)_2]^+$ (phen = 1, 10-phenathroline) had the ability to intercalate DNA and cause cleavage. Several other phen and related ligands have been coordinated to copper and studied. A significant number of the complexes have been found to exhibit reactivity similar to nucleases [60–64]. Whereas the phen and related ligands have seen more frequent applications, other planar pi systems like quinoline have attracted less attention [65,66]. We are exploring various Schiff-base ligands containing the quinoline moiety to synthesize new copper complexes and study their DNA binding and cleavage capabilities. In this study we report the synthesis of two copper complexes containing the Schiff-base ligands derived from 8-aminoquinoline. The structures of the complexes have been determined by single crystal X-ray diffraction. The reactivity of the complexes towards calf thymus-DNA (CT-DNA) and plasmid DNA has been evaluated. In addition, kinetics experiments with BNPP and 4-NPP indicate that the complexes do hydrolyze the model compounds at reasonable rates.

2. Experimental section

2.1. Reagents and materials

All chemicals were purchased commercially and used as received. Copper(II) chloride, Copper(II) acetate, 8-aminoquinoline, 1-methyl-2-imidazolecarboxaldehyde, 2-hydroxy-1-napthaldehyde, ammonium hexafluorophosphate, ethidium bromide (EB), bis(4-nitrophenyl) phosphate (BNPP) sodium salt, 4-nitrophenyl phosphate disodium salt (4-NPP), calf-thymus DNA (CT-DNA), toluene, $NaH_2PO_4{\cdot}H_2O$ and NaCl were purchased from Sigma Aldrich. Dichloromethane and methanol were purchased from Pharmco-Aaper. Plasmid DNA pBR322 DNA was purchased from Thermo Scientific. The reagents were used without further purification.

2.2. Methods and instrumentation

^1H NMR and ^{13}C NMR were recorded on a Varian 400 MHz spectrometer. A Perkin Elmer Spectrum 100 FT-IR spectrometer was used for the IR spectra. UV–Vis spectra as well as the reactivity studies and absorption titration studies were recorded on the Shimadzu UV-1700 UV–Vis spectrophotometer. Ethidium bromide competitive binding studies were performed using the Jasco-FP 750 spectrofluorimeter. Cyclic voltammetry measurements were performed using a BAS CV-50W voltammetric analyzer. A three-electrode arrangement made up of a glassy carbon working electrode, a platinum wire auxiliary electrode and a Ag/AgCl reference electrode was used. The glassy carbon electrode was polished using alumina before each use. The cyclic voltammograms were recorded in methanol or dichloromethane with tetrabutylammonium hexafluorophosphate, (TBAHP), (0.10 M) as the supporting electrolyte. The concentrations of the complexes were 5.0 mM. Initial scans of the supporting electrolyte were made for the background check. The solutions were purged with N_2(g) for 2–3 min prior to each scan. Scan rate for each measurement was 100 mV/s. Plasmid DNA cleavage analyses were performed by gel electrophoresis using a Gel Doc-IT imaging System equipped with a Hamamatsu camera. Elemental analyses for C, H and N were performed by Galbraith Laboratories, Inc. Knoxville, TN. The X-ray crystal structure determinations and ESI-MS were performed by Dr. Fook S. Tham and Mr. Ron New respectively, of the Department of Chemistry, University of California, Riverside, CA.

2.3. Synthesis of ligands

2.3.1. (E)-N-((1-Methyl-1H-imidazol-2-yl)methylene)quinolin-8-amine, MICQ

This ligand was prepared by the reaction of 1-methyl-2-imidazolecarboxaldehyde (385 mg, 3.50 mmol) and 8-aminoquinoline (500 mg, 3.50 mmol) in 30 mL toluene. The mixture was refluxed overnight. The solution was then rotary evaporated to dryness forming a brown oily product. The oily substance was purified by column chromatography. The alumina column was first eluted with dichloromethane yielding a yellow fraction. The column was then eluted with a 1:1 v/v methanol/dichloromethane solution that resulted in a brown fraction. This fraction was then covered loosely with aluminum foil and left in the fume hood for the solvent to evaporate. A brownish-yellow oil was left. This product was then dissolved in 15 mL of CH_2Cl_2 and the solution was added drop-wise into 100 mL of hexane. A light brownish-yellow precipitate was collected by vacuum filtration. Yield: 308 mg (37.3%). Elemental analysis: Found (Calc.) for $C_{14}H_{12}N_4$, C, 72.31 (71.17); H, 5.37 (5.12); N, 22.01 (23.71). FTIR data (neat, v/cm^{-1}): 3164 (w), 3145 (w), 3036 (w), 1610 (s), 1573 (m), 1504 (s), 1472 (s), 1377 (s), 1334 (s), 1280 (m), 1108 (s), 1082 (m), 1040 (w), 816 (s), 780 (s), 748 (s). ^1H NMR (400 MHz, $CDCl_3$): δ (ppm) 4.0 (3H, s), 6.92 (1H, d, J = 7.4 Hz), 7.08 (1H, s), 7.15 (1H, d, J = 8.2 Hz), 7.25 (1H, s), 7.32 (1H, t, J = 7.6 Hz), 7.35 (1H, t, J = 4.1 Hz), 8.05 (1H, dd, J = 8.4, 1.8 Hz), 8.75 (1H, dd, J = 4.3, 1.6), 9.81 (1H, s). ^{13}C NMR (400 MHz, $CDCl_3$): δ (ppm) 35.9, 110.0, 118.0, 121.5, 126.8, 127.3, 129.1, 131.0, 135.0, 135.6, 138.0, 147.4, 148.1, 182.0.

2.3.2. (E)-1-((Quinolin-8-ylimino)methyl)naphthalen-2-ol, (TL1)

2-Hydroxy-1-napthaldehyde (978 mg, 5.68 mmol) was added to a solution of 8-aminoquinoline (814 mg, 5.65 mmol) in methanol (30 mL). The mixture was refluxed for 4 h. After cooling, a yellow-orange plate like precipitate formed. The product was isolated by vacuum filtration and re-crystallized from methanol. Yield: 1.45 g (80.9%). Elemental analysis: Found (Calc.) for $C_{20}H_{14}N_2O$: C, 80.29 (80.51); H, 4.88 (4.73); N, 9.37 (9.39), FTIR data (neat, v/cm^{-1}): 3058 (w), 3040 (w), 1623 (s), 1609 (s), 1590 (s), 1533 (s), 1488 (m), 1472 (m), 1354 (s), 1299 (s), 1205(s), 1081 (m), 956 (m), 787 (s), 744 (s), 735 (s). ^1H NMR (400 MHz, $CDCl_3$): δ (ppm) 6.90 (1H, d, J = 9.6 Hz), 7.26 (1H, t, J = 8.0 Hz), 7.46 (1H, t, J = 8.4 Hz, 7.2 Hz), 7.47 (1H, d, J = 8.8 Hz), 7.51 (1H, t, J = 4.4 Hz), 7.57 (1H, d, J = 8.0), 7.63 (1H, d, J = 12.0 Hz), 7.66 (1H, t, J = 10.0 Hz, 9.6 Hz), 7.75 (1H, dd, J = 7.4 Hz, 1.4 Hz), 7.99 (1H, d, J = 7.6 Hz), 8.18 (1H, dd, J = 8.0 Hz, 1.6 Hz), 9.07 (1H, dd, J = 4.4 Hz, 1.6 Hz), 9.26 (1H, s) 9.28 (1H, s, absent upon D_2O addition), ^{13}C NMR (400 MHz, $CDCl_3$): δ (ppm) 108.76, 113.06, 118.33, 122.30, 123.62, 124.28, 126.52, 126.63, 126.72, 128.34, 128.94, 129.49, 134.19, 135.90, 137.50, 139.39, 139.90, 146.10, 150.25, 181.83.

2.4. Synthesis of [Cu(MICQ)Cl](PF$_6$) (**1**)

The ligand MICQ, (200 mg, 0.856 mmol) was dissolved in 25 mL of methanol. Copper(II) chloride (144 mg, 0.856 mmol) was dissolved in 25 mL methanol in a different flask. The copper chloride solution was then added drop-wise to the ligand solution. The mixture immediately turned a dark green color. The mixture

was heated to 60 °C for 10 min while stirring and then allowed to cool to room temperature. The precipitate was vacuum filtered, and the product washed with a small amount of cold methanol. The product was allowed to dry (212 mg recovered, 67.6% yield). Suitable crystals for structure determination were grown in deionized water with the addition of NH_4PF_6. Elemental analysis: Found (Calc.) for $C_{14}H_{12}N_4ClCuPF_6$, [Cu(MICQ)Cl](PF_6): C, 35.71 (34.99); H, 2.38 (2.52); N, 11.59 (11.66), ESI-MS: m/z = 334 $[M-PF_6^-]^+$, FTIR data (neat, v/cm^{-1}): 3126 (w), 3071 (w), 1604 (m), 1583 (m), 1505 (m), 1484 (m), 1434 (m), 1414 (m), 1392 (m), 1303 (m), 1077 (m), 827 (s), 791 (m), 760(s), 740 (s), UV–Vis: (methanol) λ_{max} 240 nm, log ε 4.18, λ_{max} 273 nm, log ε 4.20, λ_{max} 393 nm, log ε 3.65, λ_{max} 596 nm, log ε 3.36.

2.5. Synthesis of Cu(TL1)(OAc)·CH_3OH (**2**)

Copper acetate, (124 mg, 0.70 mmol) was dissolved in methanol (35.0 mL). The ligand TL1 (206 mg, 0.70 mmol) was dissolved in methanol (100 mL). The copper acetate solution was added dropwise to this solution. An immediate color change to a yellowish green solution was observed. Once all of the copper acetate solution had been added the solution was heated and stirred for 2–3 min. The solution was allowed to cool to room temperature and then refrigerated for 2 days to allow slow crystallization. The dark brown needlelike crystals were collected by vacuum filtration and washed twice with 3–5 mL aliquots of ice-cold methanol and dried under vacuum. Yield: 0.335 g (68.4%). Elemental analysis: Found (Calc.) for $C_{23}H_{20}N_2O_4Cu{\cdot}CH_3OH$: C, 60.67 (61.19); H, 4.24 (4.46); N, 6.18 (6.20), ESI-MS: m/z = 360 $[M-CH_3CO_2^-]^+$, FTIR data (neat, v/cm^{-1}): 3058, 1601, 1575, 1537, 1503, 1457, 1428, 1364, 1322, 1304, 1265, 1239, 1202, 1169, 1093, 1033, 977, 825, 746, 730, 656, UV–Vis: (methanol) λ_{max} 230 nm, log ε 6.68, λ_{max} 260 nm, log ε 4.42, λ_{max} 348 nm, log ε 3.99, λ_{max} 453 nm, log ε 4.22, λ_{max} 476 nm, log ε 4.26.

2.6. X-ray structure determination

A green thin needle-plate fragment (0.51 × 0.16 × 0.02 mm^3) was used for single crystal X-ray diffraction data for complex **1**, $[C_{14}H_{12}N_4ClCu]^+[PF_6]^-$. For complex **2** $C_{20}H_{13}N_2OCH_3COOCu{\cdot}CH_3OH$, a black prism (0.21 × 0.09 × 0.03 mm^3) was used. Each crystal was coated with paratone oil and mounted on a cryo-loop glass fiber. X-ray intensity data were collected at 100(2) K on a Bruker APEX2 [67] platform-CCD X-ray diffractometer system (fine focus tube, Mo radiation, λ = 0.71073 Å, 50 KV/30 mA power). The CCD detector was placed at a distance of 5.0400 cm from the crystal of complex **1**, and at a distance of 5.0700 cm from the crystal of complex **2**. A total of 3600 frames were collected for a sphere of reflections (with scan width of 0.3° in ω, starting ω and 2θ angles of −30°, and ϕ angles of 0°, 90°, 120°, 180°, 240°, and 270° for every 600 frames, 80 s/frame exposure time for complex **1** and 30 s/frame exposure time for complex **2**). For complex **1**, the Bruker CELL NOW program [68] was used to obtain the two different orientation matrices of the rotational twin components (Twin law is 180° rotation about the 100 real axis). These matrices were imported into the APEX2 program for Bravais lattice determination and initial unit cell refinement. The frames were integrated using the Bruker SAINT software package [69] and using a narrow-frame integration algorithm. Based on a monoclinic crystal system, the integrated frames yielded a total of 4480 unique independent reflections [R_{int} = 0.0474, maximum 2θ = 58.26° (0.73 Å resolution), data completeness = 100%] and 4064 (90.7%) reflections were greater than 2$\sigma(I)$. The unit cell parameters were, a = 14.9130(18) Å, b = 15.4330(19) Å, c = 7.2754(9) Å, β = 95.207(2)°, V = 1667.5(4) Å^3, Z = 4, D_{calc} = 1.913 g/cm^3. Absorption corrections were applied (absorption coefficient μ = 1.637 mm^{-1} maximum/minimum transmission = 0.9743/0.4867) to the raw intensity data using the Bruker TWINABS program [70]. The integrated frames for complex **2** yielded a total of 40708 reflections at a maximum 2q angle of 58.26° (0.73 Å resolution), of which 5152 were independent reflections (R_{int} = 0.0417, R_{sig} = 0.0239, redundancy = 7.9, completeness = 99.9%) and 4316 (83.8%) reflections were greater than 2$\sigma(I)$. The unit cell parameters were, a = 8.1846(2) Å, b = 17.7964(5) Å, c = 13.3740(4) Å, β = 100.701(1)°, V = 1914.13(9) Å^3, Z = 4, D_{calc} = 1.568 g/cm^3. Absorption corrections were applied (absorption coefficient μ = 1.176 mm^{-1}; maximum/minimum transmission = 0.9633/0.7937) to the raw intensity data using the SADABS program [71]. The Bruker SHELXTL software package [72] was used for phase determination and structure refinement for both complexes. The first twin domain HKL intensity data was used with the distribution of intensities (E^2-1 = 0.898 for complex **1** and E^2-1 = 0.947 for complex **2**). Systematic absent reflections indicated one possible space group, $P2(1)/c$. The space group $P2(1)/c$ (#14) was later determined to be correct for both complexes. Direct methods of phase determination followed by two Fourier cycles of refinement led to an electron density map from which most of the non-hydrogen atoms were identified in the asymmetry unit of the unit cell. With subsequent isotropic refinement, all of the non-hydrogen atoms were identified. The combined (major and minor components) HKLF 5 intensity dataset was used in the final structure refinement. There was one cation of $[C_{14}H_{12}N_4ClCu]^+$ and one anion of $[PF_6]^-$ present in the asymmetry unit of the unit cell of complex **1** and one molecule of Cu-complex, $[C_{20}H_{13}N_2O][CH_3COO]Cu$ with one solvent molecule of CH_3OH present in the asymmetric unit of the unit cell of complex **2**. The rotational twin law was 180° rotation about the 100 real axis. The major/minor twin component ratio was 57%/43%.

Atomic coordinates, isotropic and anisotropic displacement parameters of all the non-hydrogen atoms were refined by means of a full matrix least-squares procedure on F^2. The H-atoms were included in the refinement in calculated positions riding on the atoms to which they were attached. The refinement converged at R_1 = 0.0386, wR_2 = 0.0890, with intensity, $I > 2\sigma(I)$ for complex **1** and at R_1 = 0.0350, wR_2 = 0.0797, with intensity $I > 2\sigma(I)$ for complex **2**. The largest peak/hole in the final difference map was 0.781/−0.594 e Å^{-3} and 0.960/−0.470 e Å^{-3} for complexes **1** and **2**, respectively. The intermolecular hydrogen bond distances and angles for complex **2** are shown in Table 3.

2.6.1. Ethidium bromide competitive binding studies

Stock solutions of ethidium bromide and CT-DNA were prepared using a phosphate buffer (pH 7.2). The concentration of the CT-DNA solution was determined to be 15.7 × 10^{-3} M by using the molar absorption coefficient (6600 M^{-1} cm^{-1}) at 260 nm. Stock solutions of complex **1** (1.15 × 10^{-3} M) in methanol and complex **2** (4.10 × 10^{-4} M) in methanol were prepared. Appropriate dilutions of the stock solutions were made for each experiment. In a typical experiment, 2 mL of the ethidium bromide (20.0 μM) solution was transferred into a cuvette. CT-DNA (10 μL) was added to the ethidium bromide solution and equilibrated at 37 °C for 15 min. Various volumes (5–25 μL) of the complex were added to the EtBr-DNA solution. A total volume of 2.45 mL was maintained by adding additional volume of the phosphate buffer to the metal complex-EtBr-DNA solutions. Each solution was incubated at 37 °C for another 15 min. The changes in the fluorescence intensities were recorded at 600 nm over a spectra range of 540–700 nm using an excitation wavelength of 520 nm. The quenching constants (K_{sv}) were calculated for each complex using a plot of the Stern–Volmer Eq. (1):

$$I_0/I = 1 + K_{sv}[\text{complex}] \quad (1)$$

where I_0 and I represent the fluorescence intensities in the absence and presence of the complex, respectively, and [complex] represent the total concentration of the complex.

2.6.2. Absorption titration studies

The absorption titration studies were carried out using a constant concentration of 8.0×10^{-5} M of the complex. A solution of CT-DNA was made in 5.0 mM Tris–HCl/NaCl buffer (pH 7.2). CT-DNA stock solution concentration was determined to be 1.70×10^{-4} M by using the absorbance at 260 nm and the extinction coefficient at that wavelength of 6600 M^{-1} cm^{-1}. The absorption spectra of the complex in the absence and presence of increasing concentrations of CT-DNA were determined in 5.0 mM Tris–HCl/NaCl buffer (pH 7.2). The change in absorbance of the MLCT absorbance for the complex was monitored with each successive addition of CT-DNA. The spectra were recorded after 10 min incubation at 37 °C. The intrinsic binding constants K_b for complexes **1** and **2** were determined from the Eq. (2):

$$[DNA]/(\varepsilon_a - \varepsilon_f) = [DNA]/(\varepsilon_b - \varepsilon_f) + 1/(K_b(\varepsilon_b - \varepsilon_f)) \quad (2)$$

where [DNA] is the concentration of CT-DNA in base pairs, ε_a, ε_f and ε_b are the apparent absorption coefficient A_{obs}/[Cu], the extinction coefficient for the free copper complex and the extinction coefficient for the fully bound complex respectively. From the plot of $[DNA]/(\varepsilon_a - \varepsilon_f)$ versus [DNA], K_b was calculated from the ratio of the slope and the intercept.

2.6.3. DNA cleavage experiments

The DNA cleavage activity of each complex was examined using super coiled pBR322 DNA. A stock solution of complex **1** was prepared with a concentration of 4.13×10^{-4} M. 30.0 μL samples of the plasmid DNA were treated with increasing complex concentrations (2.0–70 μL) and enough buffer solution for a final volume of 100 μL. The samples were incubated in the dark for 20 h at 37 °C. The DNA cleavage experiments were analyzed by 1% agarose gel electrophoresis using 1× Tris–acetate–EDTA (TAE) running buffer. 10 μL of each reaction solution together with 2.0 μL of the loading dye was loaded into the wells and subjected to electrophoresis at 60 V for 90 min. The gel was stained with 1% ethidium bromide and documented using a Gel Doc-IT imaging system. A similar procedure was used for complex **2**.

2.7. Reactivity with BNPP and 4-NPP

The hydrolysis of BNPP and 4-NPP by complex **2** were observed by monitoring the increase in absorbance at 400 nm due to the formation of the 4-nitrophenolate ion. In a typical experiment, 2.0 mL of BNPP (2.0×10^{-3} M) or 4-NPP (2.7×10^{-3} M) in Tris–HCl buffer (pH 7.2) was transferred into a cuvette in the sample compartment of the spectrophotometer. A similar solution was placed in the reference compartment to correct for the hydrolysis in the absence of the catalyst. 1.0 mL of the buffer was added to the reference cuvette to bring the total volume to 3.0 mL. The cuvettes were equilibrated at 50.0 °C for 10 min. A solution of the complex (4.13×10^{-4} M), (1.0 mL), which had been equilibrated at 50.0 °C, was immediately added to the BNPP solution and the measurements were recorded. The observed rate constant k_{obs} were determined from the plots of $\ln(A_{inf} - A_t)$ versus time (s) where A_t is the absorbance at time t seconds and A_{inf} is the absorbance at the end of the reaction. In one experiment, complex **1** showed hydrolysis of BNPP, however this experiment for complex **1** was not reproducible.

3. Results and discussion

3.1. Synthesis and characterization

The ligands MICQ [73] and TL1 were prepared by the Schiff-base condensation reaction of 8-aminoquinoline and the corresponding aldehyde. The products were purified by column chromatography. Each ligand was characterized by use of various spectroscopic methods. Major spectroscopy features are reported in the synthesis section. Complex **1** was prepared by reacting the ligand MICQ with a methanol solution of copper(II) chloride whereas complex **2** was prepared by reacting the ligand TL1 with copper(II) acetate in methanol. Both complexes are soluble in DMF and methanol. Complex **2** is also soluble in dichloromethane. The MS of the complex showed a major cluster at m/z of 334 for the M^+, $[Cu(MICQ)]^+$ ion. The UV–Vis spectrum of MICQ in methanol has two major peaks at 250 nm and 340 nm. These peaks are assigned to the π–π^* of the ligand. The UV–Vis spectrum of complex **1** in methanol exhibits three peaks in the range 220–700 nm. The two intense peaks at λ_{max} 386.5 nm and 237.5 nm corresponded to the π–π^* absorption within the ligand. The peak at 651.0 nm corresponds to the metal–ligand charge transfer (MLCT) absorption. The ESI-MS spectrum of complex **2** showed an m/z at 360 for the $[M-OAc]^+$ ion. The electronic spectrum of complex **2** in methanol shows five peaks, three peaks in the UV region and two peaks in the visible region. The peaks in the UV region can be assigned to the π–π^* absorption within the ligand TL1, while the two lower energy bands are assigned to the MLCT bands.

3.2. Crystal structure

The crystal data and structure refinements for complexes **1** and **2** can be observed in Table 1. The crystals for complex **1** were grown by slow evaporation of an aqueous solution of $[Cu(MICQ)Cl](PF_6)$. The crystal structure of complex **1** is shown in Fig. 1. The geometry around the copper is a distorted square planar geometry with the metal coordinated to the tridentate MICQ ligand and the fourth coordination site occupied by a chlorine. The packing diagram (Fig. 2) shows a spiral staircase arrangement resulting in a penta-coordinated copper center with a chlorine ligand from another unit serving as the axial donor atom. Selected bond lengths and angles are shown in Table 2. In complex **1**, the bond lengths between the copper and the chlorine ligands are 2.248(9) Å and 2.6269(10) Å for the equatorial and the axial chlorines respectively. A similar trend has been found in other copper complexes [74]. As a consequence of the weak $Cu–Cl_{(bridging)}$ bonds such packing arrangement in complex **1** is not sustained in solution where the solvent has strong donor atoms [75]. Complex **1** and complex **2** both have identical 8-aminoquinoline rings as part of the tridentate ligand. The structure of complex **2** is shown in Fig. 3. The bond lengths around the copper center from the nitrogen donors of the 8-aminoquinoline moiety are Cu(1)–(N1), 2.002(3) Å and 1.9922(16) Å for complex **1** and complex **2** respectively. The bond lengths of the $Cu(1)–N(2)_{(imine)}$ are 1.997(2) Å and 1.9416(15) Å for complex **1** and complex **2**, respectively. In addition, complex **1** also has a $Cu(1)–N(3)_{(imidazole)}$ bond length of 1.984(3) Å. These bond lengths are comparable to similar 8-aminoquinoline Schiff base and imidazole copper complexes [51,66,74,76,77]. Complex **2** has two Cu–O bonds, with bond lengths of Cu(1)–O(1) and Cu(1)–O(2) being 1.8992(14) Å and 1.9426(13) Å, respectively. The shorter bond length being the $Cu–O_{(phenolate)}$. This shorter bond length is due to the phenolate oxygen being a stronger base than the carboxylate oxygen. The two polycyclic rings of the tridentate ligand, TL1 are approximately in the same plane. There is one

Table 1
Crystal data and structure refinement for complexes **1** and **2**.

	1	**2**
Empirical formula	$C_{14}H_{12}ClCuF_6N_4P$	$C_{23}H_{20}CuN_2O_4$
Formula weight	480.24	451.95
T (*K*)	100(2)	100(2)
λ (Å)	0.71073	0.71073
Crystal system	monoclinic	monoclinic
Space group	*P*2(1)/*c*	*P*2(1)/*c*
Unit cell dimensions		
a (Å)	14.9130(18)	8.1846(2)
b (Å)	15.4330(19)	17.7964(5)
c (Å)	7.2754(9)	13.3740(4)
α (°)	90	90
β (°)	95.207(2)	100.701(1)
γ (°)	90	90
V (Å^3)	1667.5(4)	1914.13(9)
Z	4	4
D_{calc} (Mg m^{-3})	1.913	1.568
Absorption coefficient (mm^{-1})	1.637	1.176
F(000)	956	932
Crystal size (mm)	0.51 × 0.16 × 0.02	0.21 × 0.09 × 0.03
Theta range for data collection (°)	1.90–29.13	1.93–29.13
Index ranges	$-20 \leqslant h \leqslant 20$, $0 \leqslant k \leqslant 21$, $0 \leqslant l \leqslant 9$	$-11 \leqslant h \leqslant 11$, $-24 \leqslant k \leqslant 24$, $-18 \leqslant l \leqslant 18$
Reflections collected	9514	40708
Independent reflections (R_{int})	4480 (0.0474)	5152 (0.0417)
Completeness to theta = 29.13°	100.0%	99.9%
Absorption correction	semi-empirical from equivalents	semi-empirical from equivalents
Maximum and minimum transmission	0.9743 and 0.4867	0.9633 and 0.7937
Refinement method	Full-matrix least-squares on F^2	Full-matrix least-squares on F^2
Data/restraints/parameters	4480/0/246	5152/0/276
Goodness-of-fit (GOF) on F^2	1.086	1.063
Final *R* indices [$I > 2\sigma(I)$]	$R_1 = 0.0386$, $wR_2 = 0.0890$	$R_1 = 0.0350$, $wR_2 = 0.0797$
R indices (all data)	$R_1 = 0.0474$, $wR_2 = 0.0954$	$R_1 = 0.0464$, $wR_2 = 0.0843$
Largest difference in peak and hole (e Å^{-3})	0.781 and −0.594	0.960 and −0.470

Table 2
Selected bond lengths and bond angles complexes **1** and **2**.

Complex **1**		Complex **2**	
Bond lengths (Å)			
Cl(1)–Cu(1)	2.2485(9)	Cu(1)–O(1)	1.8992(14)
Cl(1)–Cu(1)#1	2.6269(10)	Cu(1)–N(2)	1.9416(15)
Cu(1)–N(3)	1.984(3)	Cu(1)–O(2)	1.9426(13)
Cu(1)–N(2)	1.997(2)	Cu(1)–N(1)	1.9922(16)
Cu(1)–N(1)	2.002(3)		
Cu(1)–Cl(1)#2	2.6269(10)		
Bond angles (°)			
Cu(1)–Cl(1)–Cu(1)#1	115.32(4)	O(1)–Cu(1)–N(2)	92.58(6)
N(3)–Cu(1)–N(2)	80.72(10)	O(1)–Cu(1)–O(2)	90.27(6)
N(3)-Cu(1)-N(1)	161.25(11)	N(2)–Cu(1)–O(2)	176.59(6)
N(2)–Cu(1)–N(1)	80.72(11)	O(1)–Cu(1)–N(1)	173.69(6)
N(3)–Cu(1)–Cl(1)	98.58(8)	N(2)–Cu(1)–N(1)	83.41(7)
N(2)–Cu(1)–Cl(1)	158.86(9)	O(2)–Cu(1)–N(1)	93.91(6)
N(1)–Cu(1)–Cl(1)	97.76(8)		
N(3)–Cu(1)–Cl(1)#2	94.10(8)		
N(2)–Cu(1)–Cl(1)#2	97.78(8)		
N(1)–Cu(1)–Cl(1)#2	91.01(9)		
Cl(1)–Cu(1)–Cl(1)#2	103.34(3)		

Table 3
Hydrogen bonds for complex **2** [Å and °].

D–H...A	d(D–H)	d(H...A)	d(D...A)	<(DHA)
O(1S)–H(1D)...O(2)	0.80(3)	1.94(3)	2.737(2)	174(3)

Symmetry transformations used to generate equivalent atoms: $-x+1$, $-y+1$, $-z+1$.

hydrogen bond interaction in complex **2** involving the alcohol group of methanol and one of the carboxylate oxygen of the coordinated acetate.

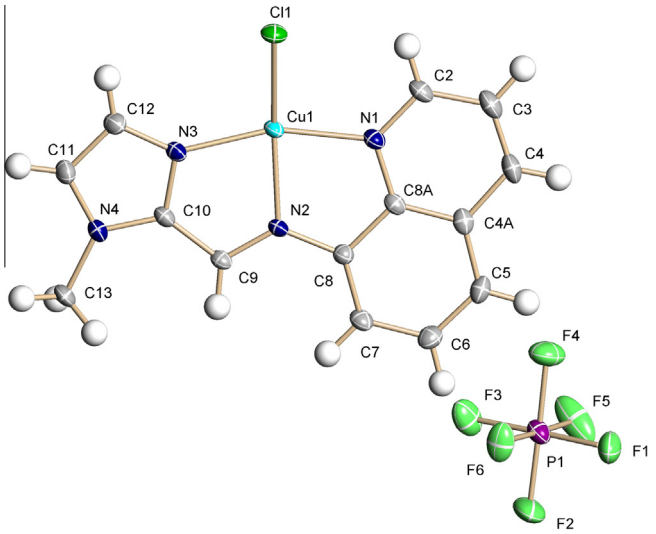

Fig. 1. Crystal structure of the complex [Cu(MICQ)Cl]PF_6 (**1**). Crystal data are given in Table 1, selected bond lengths and bond angles are in Table 2.

3.3. Electrochemistry

Cyclic voltammetry of complex **1** was performed in methanol using a glassy carbon-working electrode, a silver chloride reference electrode and a platinum wire auxiliary electrode in the potential range of +0.6 to −0.4 V. All potentials are with reference to Ag/AgCl. Fig. 4 shows a reduction peak at −0.085 V corresponding to the $Cu^{2+} \rightarrow Cu^{+}$ and a less reversible oxidation peak at 0.18 V for complex **1**. The nature of the oxidation peak suggests that Cu^{+} species is not stable in the solution. Neves and co-workers [51] have

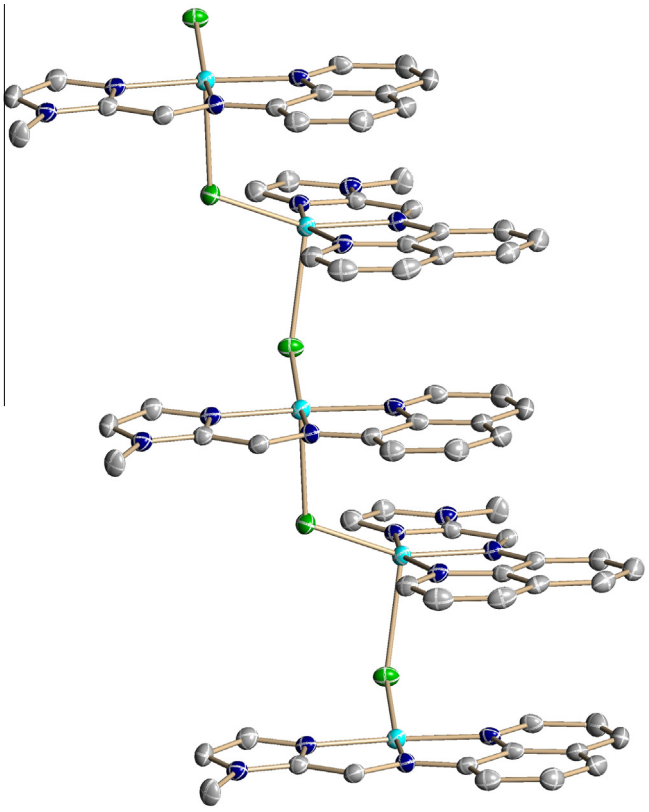

Fig. 2. Packing diagram for the complex [Cu(MICQ)Cl]PF_6 (**1**). The anion has been omitted for clarity.

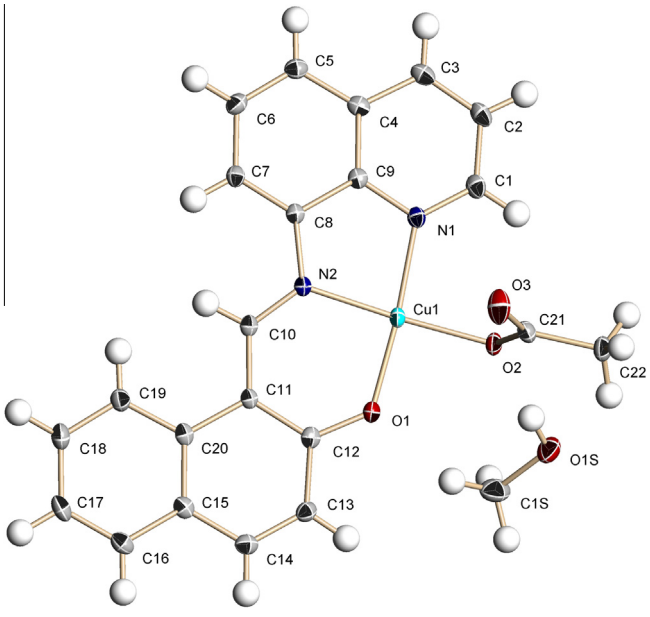

Fig. 3. Crystal structure of the complex [Cu(TL1)(OAc)]·CH_3OH (**2**). Crystal data are given in Table 1, selected bond lengths and bond angles are in Table 2.

reported similar cyclic voltammograms for their imidazole rich copper complexes. In methanol, complex **2** showed no active redox behavior in the scan range of −0.40 V to 1.60 V. The cyclic voltammogram of complex **2** (Fig. 5) was recorded in dichloromethane. The $E_{1/2}$ for complex **2** was found to be 1.482 V, which is more positive compared to values reported for similar copper complexes

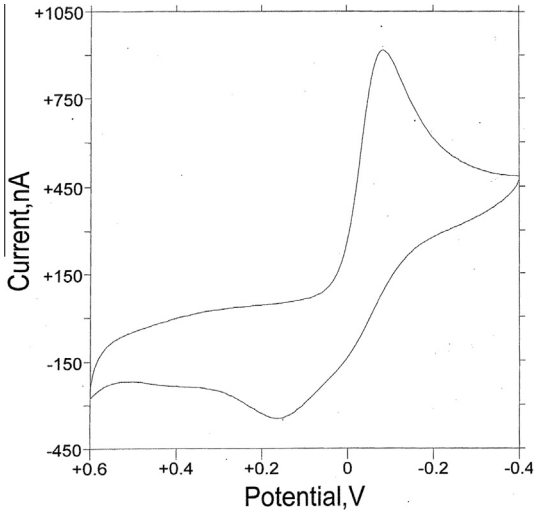

Fig. 4. Cyclic voltammogram for the complex [Cu(MICQ)Cl]PF_6 (**1**) in methanol with TBAHP (0.10 M) as the supporting electrolyte, at scan rate of 100 mV/s, potential expressed with reference to Ag/AgCl electrode.

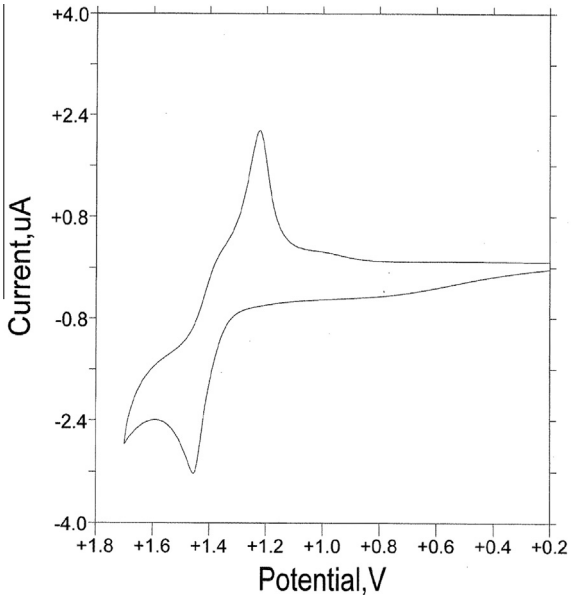

Fig. 5. Cyclic voltammogram for the complex [Cu(TL1)(OAc)]·CH_3OH (**2**) in methanol with TBAHP (0.10 M) as the supporting electrolyte, at scan rate of 100 mV/s, potential expressed with reference to Ag/AgCl electrode.

[21–23]. Whereas the cyclic voltammogram of complex **1** shows an irreversible reduction peak, the cyclic voltammogram of complex **2** shows quasi-reversible peaks. The difference in the redox potential of the complexes is a result of the structural difference of the two complexes. The much higher potential for complex **2** could be attributed to the coordination of the phenolate oxygen and the presence of the pi framework of the naphthalene group.

3.4. Reactivity of the complexes with DNA

Fluorescence spectroscopy studies were used to assess the binding abilities of the complexes with CT-DNA. Unbound ethidium bromide is weakly fluorescent, however, this ability is tremendously increased when ethidium bromide interacts with DNA. The displacement of ethidium bromide from CT-DNA and ethidium bromide bound complex by a metal complex results in

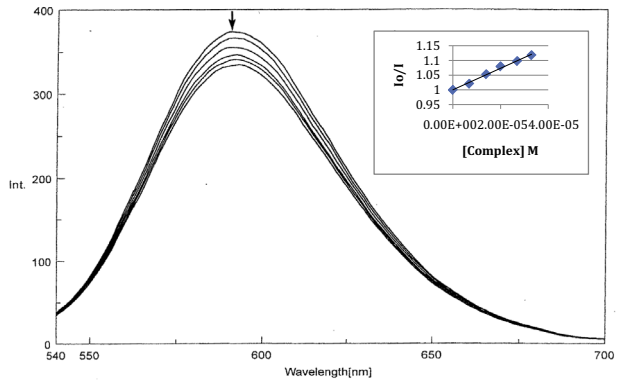

Fig. 6. Changes in the fluorescence emission spectra of CT-DNA and ethidium bromide bound complex in Tris–HCl buffer (pH = 7.2) with increasing concentration of the complex [Cu(MICQ)Cl]PF_6 (**1**). [CT-DNA] = 1.60×10^{-4} M, [EB] = 2.00×10^{-5} M, λ_{ex} = 520 nm. Inset shows the plot of emission intensity I_0/I versus [complex].

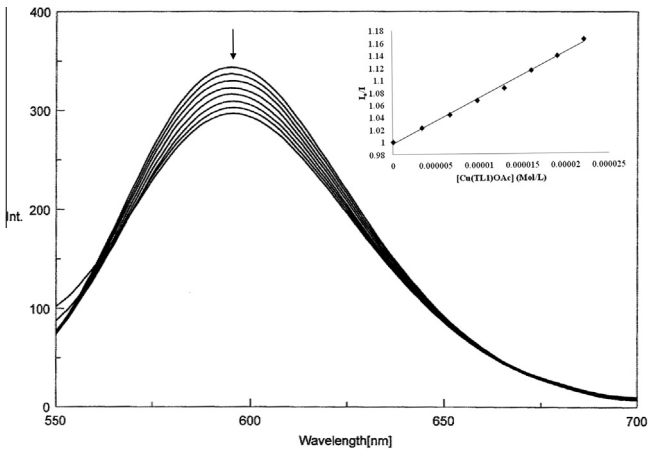

Fig. 7. Changes in the fluorescence emission spectra of CT-DNA and ethidium bromide bound complex in Tris–HCl buffer (pH = 7.2) with increasing concentration of the complex [Cu(TL1)(OAc)]·CH_3OH (**2**), [CT-DNA] = 1.60×10^{-4} M, [EB] = 2.00×10^{-5} M, λ_{ex} = 520 nm. Inset shows the plot of emission intensity I_0/I versus [complex].

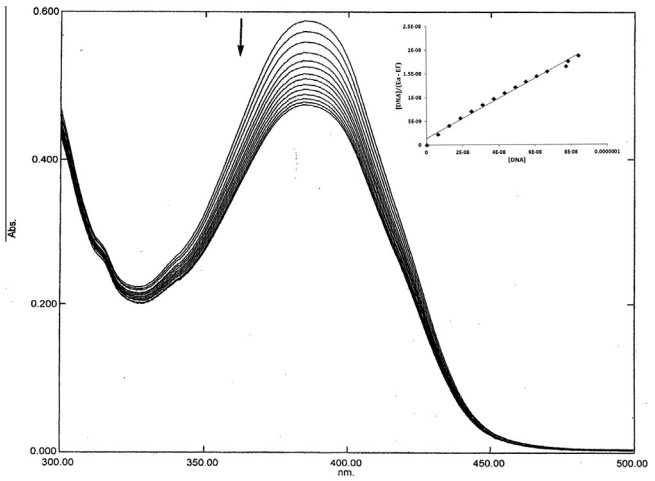

Fig. 8. Absorption spectra of the complex [Cu(MICQ)Cl]PF_6 (**1**) in the absence and presence of increasing concentrations of CT-DNA (0–84.3 μM) at 37 °C. The inset shows the plot of [DNA]/($\varepsilon_a - \varepsilon_f$) versus [DNA].

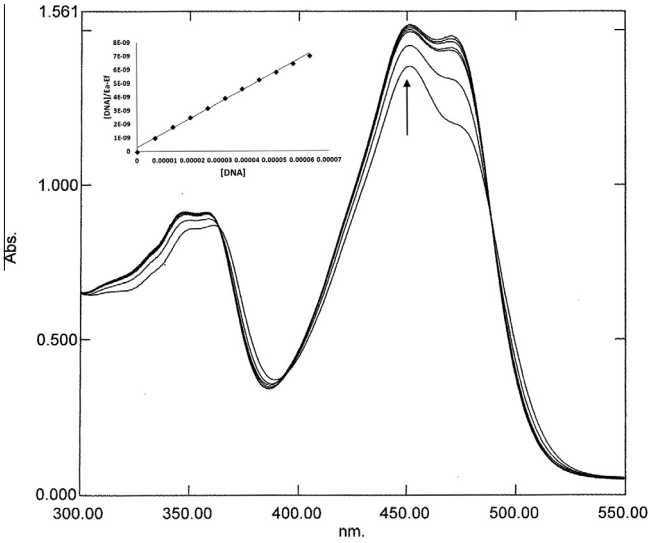

Fig. 9. Absorption spectra of the complex [Cu(TL1)(OAc)]·CH_3OH (**2**) in the absence and presence of increasing concentrations of CT-DNA (0–84.3 μM) at 37 °C. The inset shows the plot of [DNA]/($\varepsilon_a - \varepsilon_f$) versus [DNA].

the decrease in the emission intensity of the CT-DNA and ethidium bromide bound complex. The accepted conclusion from such studies is that the metal complex preferentially and strongly binds to the CT-DNA compared to ethidium bromide through intercalation. Figs. 6 and 7 show changes in the emission spectra observed upon the addition of solution of complex **1** and complex **2** respectively to a solution of CT-DNA and ethidium bromide bound complex. In both cases, the observed trend is a decrease in the emission intensity with increasing concentration of the complex. These observations are in good agreement with the Stern–Volmer expression. The Stern–Volmer quenching plot of I_0/I versus concentration of the copper complex gave K_{sv} values of 3.70×10^3 M^{-1} and 7.82×10^3 M^{-1} for complexes **1** and **2**, respectively. The K_{sv} value for complex **2** is approximately twice the value for complex **1** indicating stronger binding by complex **2**. Structurally, complex **2** contains more planar polycyclic rings than complex **1**. Complexes with planar polycyclic rings as part of the ligand moiety have been found to be good DNA intercalators [54–58,60].

The reactivity of the complexes with DNA was also studied through absorption titration by monitoring the absorbance changes at 383 nm for complex **1** and 453 nm for complex **2**, upon addition of increasing amounts of DNA to a fixed amount of the complex. The absorption spectra of complex **1** (Fig. 8) in the presence of CT-DNA displayed a hypochromic shift whereas the absorption spectra of complex **2** (Fig. 9) showed a hyperchromic shift. The increase in absorbance for complex **2** is an indication for minor groove binding of the complex to DNA [74]. The intrinsic binding constant for each complex was determined from the plot of [DNA]/($\varepsilon_a - \varepsilon_f$) versus [DNA]. The ratio of the slope and intercept from gave intrinsic binding constant K_b of 1.52×10^5 M^{-1} for complex **1** and K_b of 5.0×10^5 M^{-1} for complex **2**. The K_b values also suggest a stronger binding affinity of complex **2** for DNA compared with complex **1**. This result supports the earlier suggestion that the difference in the K_{sv} values could be attributed to the extra planar ring in complex **2** resulting in stronger binding of complex **2** to the DNA. It is noteworthy to mention that the K_b values obtained for complex **1** and complex **2** are about ten times greater than the value reported for the DNA intercalator complex [Ru(phen)$_2$(dpq)]$^{2+}$. A K_b value of 1.41×10^5 M^{-1} has been reported for some copper complexes [76].

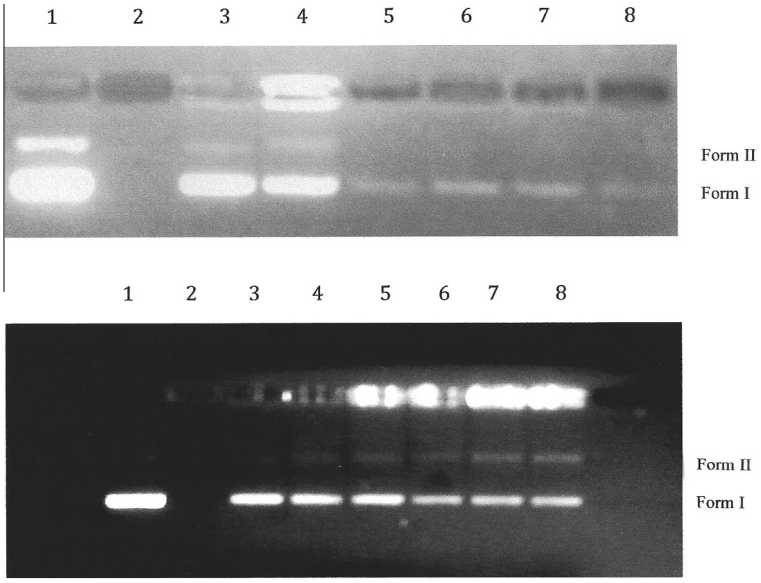

Fig. 10. Agarose gel electrophoresis analysis of the cleavage of SC pBR322 DNA by complex **1** (top) and complex **2** (bottom) at increasing concentrations of the complexes. Lane 1 DNA only, Lane 2: metal complex only, Lane 3: DNA + 0.04, Lane 4: DNA + 0.08, Lane 5: DNA + 0.12, Lane 6: DNA + 0.16, Lane 7: DNA + 0.20, Lane 8: DNA + 0.25 mM of complex.

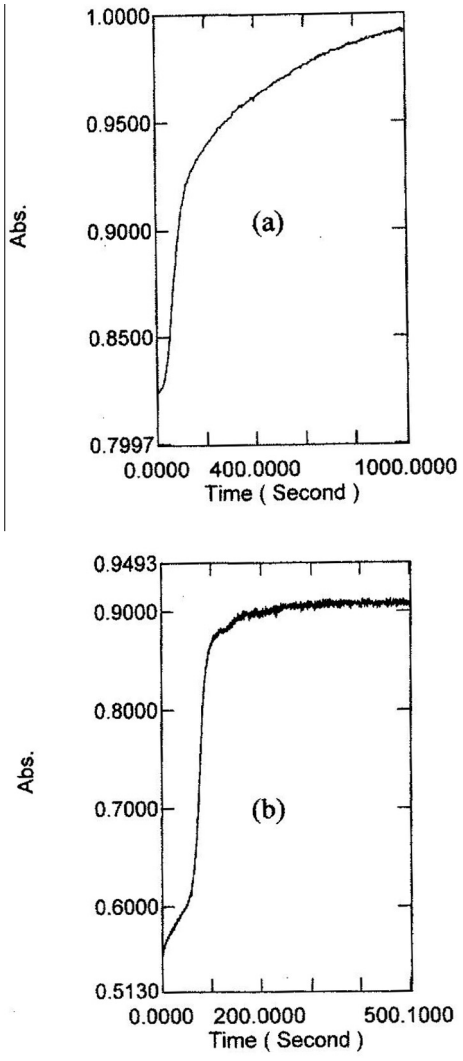

Fig. 11. Absorbance versus time (s) plot for the hydrolysis of (a) BNPP (2.15 mM) and (b) 4-NPP (2.10 mM) in Tris–HCl buffer (pH = 7.2) by the complex [Cu(TL1)(OAc)]·CH_3OH (**2**) (0.45 mM) in methanol at 37 °C. Absorbance monitored at λ_{max} 400 nm.

3.5. Plasmid DNA cleavage studies

The gel electrophoresis studies make it possible for the separation of the various forms of the DNA after cleavage. Generally, the super-coiled DNA, form **I**, has a greater mobility than the open-circular DNA, form **II** as a result of the differences in the shape to charge ratio. Cleavage of the super-coiled DNA, form **I**, produces the open-circular DNA, form **II**. The agarose gel electrophoresis analysis indicated that both complex **1** and complex **2** exhibit cleavage activities towards plasmid DNA. As can be seen from Fig. 10, cleavage of the plasmid DNA increased as the concentrations of the metal complexes were increased resulting in corresponding decrease in the intensity of form **I**.

3.6. BNPP and NPP hydrolysis

The hydrolysis of the model phosphate ester compound as BNPP is an efficient procedure to probe the hydrolytic properties of metal complexes. The hydrolysis of BNPP produces the 4-nitophenolate ions that were monitored spectrophotometrically at 400 nm. Fig. 11 shows the absorbance versus time plot for the reaction of complex **2** with BNPP. An observed rate constant of $1.43 \times 10^{-2}\ s^{-1}$ was calculated for the reaction of complex **2** with BNPP. A similar reaction using complex **2** and 4-NPP was carried out. Interestingly, the observed rate constant was determined to be $8.01 \times 10^{-2}\ s^{-1}$, which is about six times faster than that determined for the BNPP reaction.

4. Conclusion

Two copper complexes have been synthesized and characterized by spectroscopic and electrochemical methods. In addition, the crystal structures of the complexes have been determined which show the coordination of the tridentate ligands to the copper center. In complex **1** a chloride ligand completes the coordination sphere whereas in complex **2** an acetate ligand occupies the fourth coordination site. In both complexes the coordination around the copper center for each molecular unit is pseudo square planar. However, in complex **1** the packing diagram shows the each copper atom is coordinated to a chloride ligand from another molecular unit. This representation results in a square-based pyra-

midal arrangement for complex **1**. The reaction of complexes **1** and **2** with CT-DNA were studied by emission spectra and UV–Vis absorption. The results of these studies suggest that both complexes strongly interact with CT-DNA. In addition, both complexes also promote plasmid pBR322 DNA cleavage. Furthermore, complex **2** was found to hydrolyze BNPP and 4-NPP. We observed differences in reactivity towards DNA by the two complexes. Since both complexes contain 8-aminoquinoline groups, the differences in reactivity towards DNA could be reasonably attributed to the presence of the naphthalene moiety in complex **2**.

Acknowledgements

The authors thank the University of Redlands for providing the funding for this work. Many thanks also to Dr. Fook Tham and Mr. Ron See of University of California, Riverside, CA for determining the single crystal X-ray structures and the ESI-MS, respectively.

Appendix A. Supplementary material

CCDC 800315 and 900831 contain the supplementary crystallographic data for complexes **1** and **2**. These data can be obtained free of charge from The Cambridge Crystallographic Data Centre via www.ccdc.cam.ac.uk/data_request/cif. Supplementary data associated with this article can be found, in the online version, at http://dx.doi.org/10.1016/j.ica.2014.12.034.

References

[1] C.G. Hartinger, S. Zorbas-Seifried, M.A. Jakupec, B. Kynast, H. Zorbas, B.K. Keppler, J. Inorg. Biochem. 100 (2006) 891.
[2] C.X. Zhang, S.J. Lippard, Curr. Opin. Chem. Biol. 7 (2003) 481.
[3] M. Groessl, E. Reisner, C.G. Hartinger, R. Eichinger, O. Semenova, A.R. Timerbaev, M.A. Jakupec, V.B. Arion, B.K. Keppler, J. Med. Chem. 50 (2007) 2185.
[4] S.J. Tan, Y.K. Yan, P.P. Lee, K.H. Lim, Future Med. Chem. 2 (2010) 1591.
[5] P.C.A. Bruijnincx, P.J. Sadler, Curr. Opin. Chem. Biol. 12 (2008) 197.
[6] E.R. Jamieson, S.J. Lippard, Chem. Rev. 99 (1999) 2467.
[7] E.I. Solomon, D.E. Heppner, E.M. Johnston, J.W. Ginsbach, J. Cirera, M. Qayyum, M.T. Kieber-Emmons, C.H. Kjaergaard, R.G. Hadt, L. Tian, Chem. Rev. 114 (2014) 3659.
[8] (a) D. Chen, Q.C. Cui, Q.P. Dou, Cancer Res. 66 (2006) 10425;
(b) C. Cen, D. Brayton, B. Shahandeh, F.L. Meyskens, P.J. Farmer, J. Med. Chem. 47 (2004) 6919;
(c) L. Giovagnini, S. Sitran, M. Montopoli, L. Caparrotta, M. Corsini, C. Rosani, P. Zanello, Q.P. Dou, D. Fregona, Inorg. Chem. 47 (2008) 6336.
[9] V.M. Manikandamathavan, V. Rajapandian, A.J. Freddy, T. Weyhermuller, V. Subramanian, B.U. Nair, Eur. J. Med. Chem. 57 (2012) 449.
[10] S. Dhar, M. Nethaji, A.R. Chakravarty, Inorg. Chem. 45 (1050) (2006). 11043-1.
[11] C. Marzano, M. Pellei, F. Tisato, C. Santini, Anticancer Agents Med. Chem. 9 (2009) 15.
[12] V. Uma, M. Elango, B.U. Nair, Eur. J. Inorg. Chem. (2007) 3484.
[13] P.U. Maheswari, K. Lappalaien, M. Sfregola, S. Barends, P. Gamez, U. Tureinen, I. Mutikainen, G.P. van Wezel, J. Reedijk, Dalton Trans. (2007) 3676.
[14] A. Pal, B. Biswas, S.K. Mondal, C.-H. Lin, R. Ghosh, Polyhedron 31 (2012) 671.
[15] Q. Wang, Z. Yu, Q. Wang, W. Li, F. Gao, S. Li, Inorg. Chim. Acta 383 (2012) 230.
[16] S.S. Massoud, R.S. Perkins, K.D. Knierim, S.P. Comiskey, K.H. Otero, C.L. Michel, W.M. Juneau, J.H. Albring, F.A. Mautner, W. Xu, Inorg. Chim. Acta 399 (2013) 177.
[17] M. Tabatabaee, M. Bordbar, M. Ghassemzadehh, M. Tahriri, M. Tahrir, Z.M. Lighvan, B. Neumuller, Eur. J. Med. Chem. 70 (2013) 364.
[18] D. Li, J. Tian, Y. Kou, F. Huang, G. Chen, W. Gu, X. Liu, D. Liao, P. Cheng, S. Yan, Dalton Trans. (2009) 3574.
[19] A. Solanki, S.B. Kumar, A.A. Doshi, C.R. Prabha, Polyhedron 63 (2013) 147.
[20] P. Kumar, B. Baidya, S.K. Chaturvedi, R.H. Khan, D. Manna, B. Mondal, Inorg. Chim. Acta 376 (2011) 264.
[21] Q. Wang, Z. Yu, Q. Wang, W. Li, F. Gao, S. Li, Inorg. Chim. Acta 383 (2012) 230.
[22] P. Rabindra, N. Raju, Polyhedron 44 (2012) 1.
[23] Y.-C. Liu, J.-H. Wei, Z.-F. Chen, M. Liu, Y.-Q. Gu, K.-B. Huang, Z.-Q. Li, H. Liang, Eur. J. Med. Chem. 69 (2013) 554.
[24] B.-T. Ko, C.-C. Chang, S.-L. Lai, F.-J. Lai, C.-C. Lin, Polyhedron 45 (2012) 49.
[25] G.-Y. Li, K.-J. Du, J.-Q. Wang, J.-W. Liang, J.-F. Kou, X.-J. Hou, L.-N. Ji, H. Chao, J. Inorg. Biochem. 119 (2013) 43.
[26] S.S. Bhat, A.A. Kumbhar, H. Heptullah, A.A. Khan, V.V. Gobre, S.P. Gejji, V.G. Puranik, Inorg. Chem. 50 (2011) 545.
[27] A. Barve, A. Kumbhar, M. Bhat, B. Joshi, R. Butcher, U. Sonawane, R. Joshi, Inorg. Chem. 48 (2009) 9120.
[28] C. Rajarajeswari, R. Longanathan, M. Palaniandavar, E. Suresh, A. Riyasdeen, M.A. Akbarsha, Dalton Trans. 42 (2013) 8347.
[29] S. Sathiyaraj, K. Sampath, G. Raja, R.J. Butcher, S.K. Gupta, Inorg. Chim. Acta 406 (2013) 44.
[30] V.M. Manikandamathavan, B.U. Nair, Eur. J. Med. Chem. 68 (2013) 244.
[31] L. Giovagnini, S. Sitran, M. Montopoli, L. Caparrotta, M. Corsini, C. Rosani, P. Zanello, Q.P. Dou, D. Fregona, Inorg. Chem. 47 (2008) 6336.
[32] P.U. Maheswari, M. van der Ster, S. Smulders, S. Barends, G.P. van Wezel, C. Massera, S. Roy, H. den Dulk, P. Gamez, J. Reedijk, Inorg. Chem. 47 (2008) 3719.
[33] A. Kumar, J.P. Chinta, A.K. Ajay, M.K. Bhat, C.P. Rao, Dalton Trans. 40 (2011) 10865.
[34] S. Ramakrishnan, D. Shakthipriya, E. Suresh, V.S. Periasamy, M.A. Akbarsha, M. Palniandavar, Inorg. Chem. 50 (2011) 6458.
[35] M. Alagesan, N.S.P. Bhuvanesh, N. Dharmaraj, Dalton Trans. 42 (2013) 7210.
[36] S. Kashanian, M.M. Khodael, H. Roshanfekr, N. Shahabadi, A. Rezvani, G. Mansouri, DNA Cell Biol. 30 (2011) 287.
[37] R. Loganathan, S. Ramakrishnan, E. Suresh, A. Riyasdeen, M.A. Akbarsha, M. Palaniandavar, Inorg. Chem. 51 (2012) 5512.
[38] S. Ishida, F. McCormick, K. Smith-McCune, D. Hannahan, Cancer Cell 17 (2010) 574.
[39] W. Zhou, X. Wang, M. Hu, C. Zhu, Z. Guo, Chem. Sci. 5 (2014) 2761.
[40] (a) G. Pratviel, J.B. Meunier, Adv. Inorg. Chem. 45 (1998) 251;
(b) S. Anbu, M. Kandaswamy, Inorg. Chim. Acta 385 (2012) 45.
[41] C. Liu, M. Wang, T. Zhang, H. Sun, Coord. Chem. Rev. 248 (2004) 147.
[42] J. Suh, Acc. Chem. Res. 25 (1992) 273.
[43] M.J. Jedrzejas, P. Setlow, Chem. Rev. 101 (2001) 608.
[44] P. Molenvald, J.F.J. Engbersen, D.N. Reinhouldt, Chem. Soc. Rev. 29 (2000) 75.
[45] L. Zhu, O. dos Santos, C.W. Koo, M. Rybstein, L. Pape, J.W. Canary, Inorg. Chem. 42 (2003) 7912.
[46] L. Tjioe, A. Meininger, T. Joshi, L. Spiccia, B. Graham, Inorg. Chem. 50 (2011) 4327.
[47] K.M. Deck, T.A. Tseng, J.N. Burstyn, Inorg. Chem. 41 (2002) 669.
[48] M.J. Belousoff, L. Tjioe, B. Graham, L. Spiccia, Inorg. Chem. 47 (2008) 8641.
[49] L. Tjioe, T. Joshi, J. Brugger, B. Graham, L. Spiccia, Inorg. Chem. 50 (2011) 621.
[50] E.L. Hegg, S.H. Mortimore, C.L. Cheung, J.E. Huyett, D.R. Powell, J.N. Burstyn, Inorg. Chem. 38 (1999) 2961.
[51] M. Scarpellini, A. Neves, R. Homer, A.J. Bortouzzi, B. Szpoganics, C. Zucco, R.A. Nome, Inorg. Chem. 42 (2003) 8353.
[52] F.H. Fry, A.J. Fischmann, M.J. Belousoff, L. Spiccia, J. Brugger, Inorg. Chem. 44 (2005) 941.
[53] (a) J. He, J. Sun, Z.-W. Mao, L.-N. Ji, H. Sun, J. Inorg. Biochem. 103 (2009) 851;
(b) S. Dhar, P.A.N. Reddy, A.R. Chakravarty, Dalton Trans. (2004) 697;
(c) B. Selvakumar, V. Rajendiran, P.U. Maheswari, H. Stoeckli-Evans, M. Palaniandavar, J. Inorg. Biochem. 100 (2006) 316.
[54] A.M. Thomas, M. Nethaji, S. Mahadevan, A.R. Chakravarty, J. Inorg. Biochem. 94 (2003) 171.
[55] L.T. Ellis, D.F. Perkins, P. Turner, T.W. Hambley, Dalton Trans. (2003) 2728.
[56] W. Xu, X. Yang, L. Yang, Z.-L. Jia, L. Wei, F. Liu, G.-Y. Lu, New J. Chem. 34 (2010) 2654.
[57] M. Tian, H. Ihmels, E. Brotz, Dalton Trans. 39 (2010) 8195.
[58] A. Kumar, J.P. Chinta, A.K. Ajay, M.K. Bhat, C.P. Rao, Dalton Trans. 40 (2011) 10865.
[59] K.A. Reich, L.E. Marshal, D.R. Graham, D.S. Sigman, J. Am. Chem. Soc. 103 (1981) 3582.
[60] Z. Molphy, A. Prisecaru, C. Slator, N. Barron, M. McCann, J. Colleran, D. Chandran, N. Gathergood, A. Kellett, Inorg. Chem. 53 (2014) 5392.
[61] A. Kellett, M. O'Connor, M. McCann, M. McNamara, P. Lynch, G. Rosair, V. McKee, B. Creaven, M. Walsh, S. McClean, A. Foltyn, D. O'Shea, O. Howe, M. Devereux, Dalton Trans. 40 (2011) 1024.
[62] A.K. Patra, S. Dhar, M. Nethaji, A.R. Chakravarty, Dalton Trans. (2005) 896.
[63] J. Madureira, C.I.V. Ramos, M. Marques, C. Maia, B. de Sousa, L. Campino, M.G. Santana-Marques, N. Farrell, Inorg. Chem. 52 (2013) 8881.
[64] P.P. Silva, W. Guerra, J.N. Silveira, A.M. da C. Ferreira, T. Bortolotto, F.L. Fischer, H. Terenzi, A. Neves, E.C. Pereira-Maia, Inorg. Chem. 50 (2011) 6414.
[65] S. Nayak, P. Gamez, B. Kozlevcar, A. Pevec, O. Robeau, S. Dehnen, J. Reedijk, Polyhedron 29 (2010) 2291.
[66] B.-T. Ko, C.-C. Chang, S.-L. Lai, C.-C. Lin, Polyhedron 45 (2012) 49.
[67] Bruker, APEX 2, version 2010.3-0, Bruker AXS Inc., Madison, Wisconsin, USA, 2010.
[68] Bruker, CELL_NOW, version 2008/2, Bruker AXS Inc., Madison, Wisconsin, USA, 2008.
[69] Bruker, SAINT, version V7.60A, Bruker AXS Inc., Madison, Wisconsin, USA, 2009.
[70] Bruker, TWINABS, version 2008/2, Bruker AXS Inc., Madison, Wisconsin, USA, 2008.
[71] Bruker, SADBAS, version 2008/1, Bruker AXS Inc., Madison, Wisconsin, USA, 2008.
[72] Bruker, SHELXTL, version 2008/4, Bruker AXS Inc., Madison, Wisconsin, USA, 2008.
[73] During the preparation of this manuscript, the reaction of 1-methyl-2-imidazolecarboxaldehyde and 8-aminoquinoline was reported: S. Mandal, D.K. Poria, D.K. Seth, P.S. Ray, P. Gupta, Polyhedron 73 (2014) 12.
[74] J. Lu, Q. Sun, J.-L. Li, L. Jiang, W. Gu, X. Liu, J.-L. Tian, S.-P. Yan, J. Inorg. Biochem. 137 (2014) 46.
[75] I. Lumb, M.S. Hundal, M. Corbella, V. Gomez, G. Hundal, Eur. J. Inorg. Chem. (2013) 4799.
[76] P. Kumar, S. Gorai, M.K. Santra, B. Mondal, D. Manna, Dalton Trans. 41 (2012) 7573.
[77] H. Liu, F. Gao, D. Niu, J. Tian, Inorg. Chim. Acta 362 (2009) 4179.